The Nature of the Optical "Jets" in the Spiral Galaxy NGC 1097

Ann E. Wehrle

Infrared Processing and Analysis Center, Jet Propulsion,

California Institute of Technology

William C. Keel[1]

Dept. of Physics and Astronomy, University of Alabama

Dayton L. Jones

Jet Propulsion Laboratory, California Institute of Technology

Received _____; accepted _____

[1] Visiting Astronomer, Cerro Tololo Inter-American Observatory, National Optical Astronomy Observatories, which is operated by AURA, Inc. under cooperative agreement with the National Science Foundation; and at the European Southern Observatory, La Sills, Chile.

ABSTRACT

We present new observations of the jet features inthebarred spiral galaxy NGC 1097, including optical spectroscopy of the brightest jet features, two-color optical imagery, new VLA mapping at 327 MHz, and archival **1.4** GHz VLA data reprocessed for improved sensitivity. No optical emission lines appear to an equivalent width limit of 15-30 Å (depending on the line wavelength). The jets are uniformly blue, with B - V = 0.45 for the two well-observed jets R1 and R2. No radio emission from the jets is detected at either frequency; the 327-MHz data set particularly stringent limits on "fossil" emission from aging synchrotrons electrons. The morphology of the jets is shown to be inconsistent with any conical distribution of emission enhanced by edge-brightening; their combination of transverse profile and relative narrowness cannot be reproduced with cone models. The optical colors, lack of radio emission, and morphology of the features lead us to conclude that they are tidal manifestations, perhaps produced by multiple encounters of the small elliptical companion NGC 1097A with the disk of NGC 1097. We present photometric and morphological comparisons to the tail of NGC 4651, which is similar in scale and morphology to the northeast "dogleg" feature RI in NGC 1097.

Subject headings: galaxies: individual (NGC 1097) — galaxies: jets — galaxies: interactions — galaxies: spiral — jets: optical

1. Introduction

The four faint optical jets emanating from the barred spiral galaxy NGC 1097 have puzzled astronomers since their discovery (Wolstencroft and Zealey 1975; Arp 1976; Lorre 1978; Carter, Allen and Malin 1984; hereafter CAM). The 15-arcsec wide jets extend radially 5'- 19' from the nucleus. No radio emission has been detected from the jets (Wolstencroft, Tully and Perley 1984; Hummel, van der Hulst and Keel 1987; hereafter WTP and HHK) although the center has been well-imaged by the VLA both in the continuum (HHK) and at the 21-cm HI line (Ondrechen, van der Hulst, and Hummel 1989). Unlike the optical features near active radio galaxies studied by McCarthy et al. (1987) and Baum and Heckman (1989a, 1989b) which have strong emission-line filaments, the optical jets of NGC 1097 lack emission lines (Arp, cited in Wolstencroft 1981; Wolstencroft, private communication; also this work). The nucleus itself has usually been observed to be a LINER or weak Seyfert 2 surrounded by an extremely luminous star formation ring within the bar (HHK and references therein). The ring of star formation, and perhaps the presence of the bar, may be related to tidal interaction with NCC 1097A, a small elliptical galaxy believed to be responsible for distortions in the optical spiral arms and HI distribution. Evidence for Seyfert 1 nuclear activity appeared unexpectedly in 1991, when Storchi-Bergmann, Baldwin, and Wilson (1993) found that a double-peaked broad-line region had appeared, possibly caused by a real luminosity flare or variable obscuration effect (see also Storchi-Bergmann et al. 1995).

We use nomenclature for the jets following Lorre (1978) with jets Rl, R2, R3, and R4 having position angles 54°, 15", 195°, and 223° respectively. All four jets are roughly linear with one jet (R1) terminating in a right angle bend, giving a '(dogleg" appearance. Lines drawn along each jet do not cross at the nucleus, but very close to it; they are not *exactly* radial. While the jets are optically faint, the dogleg jet can easily be seen on an ESO-SRC

J film copy.

Four observations have been used to constrain the nature of the jets: first, the lack of emission features in the optical spectrum (Wolstencroft 1981), second, an upper limit to the x-ray emission (Wolstencroft et al. 1983; hereafter WKAS), third, the non-detection of radio emission from the jets (HHK and WTP), and fourth, the steepness of the optical-near-infrared spect rum (CAM). The optical spectrum (as j udged from the broad-band continuum color, no spectral features having been detected) could be produced bystars or bya plasma at 10^6 K via thermal (free-free) emission, as proposed by WTP. WTP excludeda synchrotron origin for thejet features because they did not detect thejets with the VLAusinga3"x 1,5" beam at 1.4 GHz (detection limit 7x10-7 Jy/sq arcsec) nor did HHK detect any emission on a scale of 15" at 1.4 GHz (detection limit of 5 $\times 10^{-6}$ Jy/sq arcsec). In addition, the optical-near-infrared colors of the dogleg jet are consistent with a typical spiral galaxy stellar population (CAM). The near-infrared emission of the dogleg jet would have to be four-to-six times weaker to provide the flat spectral index expected from free-free emission generated by a plasma of temperature 10^6 K, as proposed by WTP.

The evidence from earlier work is fairly convincing that the optical jets are composed of stars. There are two possible origins: the stars formed in situ by matter entrained by relativistic jets, or they are tidal remnants of galactic interaction. We searched for optical emission lines (as from HII regions) and obtained optical colors to put an upper limit on the stellar age, which we could use to date a possible starburst triggered either by the passage of relativistic jets or by tidal interaction in a merger. Alternatively, the colors can be used to date stars which were torn from NGC 1097 (or its merging partner) if the jets are actually tidal debris. We also obtained optical images to characterize the profile of the dogleg jet (R1) to determine if it had the asymmetry characteristic of the edge of a cone (whose sides would be jets R1 and R2).

The early radio work did not rule out the possibility that currently inactive synchrotrons jets had produced radio lobes in the past. Such lobes would fade by synchrotrons losses and adiabatic expansion after energy injection ceased. If we assume that NCC 1097 once had radio lobes similar to those of weak radio galaxies, namely, an initial radio spectral index a of -0.75 ($S_\nu \propto \nu^\alpha$) and a magnetic field strength of 10 μGauss, then the break in the synchrotrons spectrum would be at 327 MHz after about 30 million years (after energy injection ceased) with a final spectral index α = -2.0 at higher frequencies. We searched for radio emission at 327 and 1465 MHz to constrain the spectral index and brightness of possible "fossil" radio lobes.

In Section 2 we describe the observations. We present our analyses in Section 3, in several cases putting earlier arguments on a more quantitative footing, and discuss the implications in Section 4. We present our conclusions in Section 5. In this paper we assume that the distance to NGC 1097 is 12.3 Mpc, using Ho = 100 km s^{-1} Mpc^{-1}; this gives a scale of **1' = 3.7** kpc.

2. Observations

2.1. Optical **Images and Spectroscopy**

Images of three of the four jets in NGC 1097 were obtained with the CTIO 4-m telescope and RCA prime-focus CCD camera. Standard B and V filters were used, with a field size of 2.4 by 4.1 arcminutes at 0.50 arcsecond/pixel (284 x 492 usable pixels). One field for each of two jets (R2 and R3) was observed (for the southern jet R3 in B only) while two partially overlapping fields were used to cover the dogleg jet RI. For the V images, fringing due to λ5577 night-sky emission was removed with interactively-scaled subtraction of a facility "library" fringe-pattern frame. Photometric calibration used Graham's (1982)

E-region standards and mean extinction values. NGC 1097 passes within 5' of the zenith at CTIO, so the airmasses are quite low. The targeted fields and exposures are listed in Table 1.

EDITOR: PLACE TABLE 1 HERE.

The fields imaged with the CCD are outlined on a copy of the SRC J survey image in Figure 1.

EDITOR: PLACE FIGURE 1 HERE.

Peak surface brightnesses were extracted, after summing across the jet profiles and excluding the brighter condensations in RI, as follows: RI, Σ_B = 26.2, Σ_V = 25.7 magnitude arcsec^{-2}; R1 dogleg region, Σ_B = 26.6, Σ_V = 26.0 magnitude arcsec^{-2}; and R2, Σ_B = 26.7, Σ_V = 26.2 magnitude arcsec^{-2}.

The absolute field positions (and registration with respect to the radio data) were determined via a local network of 44 star positions measured from a glass copy of the SRC J survey plate, using the two-axis Grant machine at NOAO. The error in the reference frame so defined, based on the scatter of positions from nearby SAO stars, is σ = 0.6 arcsecond.

In Figure 2 we show the mosaicked B image of the northeast jet R1. The mosaic has had exposure-time differences removed by normalization,

EDITOR: PLACE FIGURE 2 HERE.

The V images of the north jet, R2, before and after convolution with a Gaussian kernel of 5" FWHM are shown in Figures 3a and 3b. The north jet (which is just east of the bright star centered in the frame), is narrower than the dogleg jet R1 (5-10" vs. 15"). There are

two other filamentary structures visible on the V image which may be real. The area near the bottom of the CCD frame where the jet R2 leaves the galactic disk is fairly smooth: the galactic disk is unperturbed.

EDITOR: PLACE FIGURE 3 HERE.

Spectroscopy was attempted for the two bright condensations in the northeast jet R1 (as indicated in Figure 2) and the northern jet R2, using the SIT-Vidicon detector on the Ritchey-Chretien spectrograph at the CTIO 4m telescope on 1 and2 October 1983. Exposures of 1-2 hours per object were obtained, covering the wavelength range 4000-7000 Å, under photometric conditions with good seeing. Thecontinuum wasdetected only very weakly (by summing across large wavelength bins) while no narrow emission lines that could contribute more than a few per cent of the broad-band intensity were seen. This adds to the existing report (Arp, cited in Wolstencroft 1981) that the jets have no emission-line features. Our limits are the following, For the brighter condensation in R1, any emission in the vicinity of $H\alpha$ at the galaxy redshift must have an equivalent width less than 15 Å, and any emission in the $H\beta$-[O III] region must fall below 30 Å. For the more diffuse condensation 2, the limits are about 2,2 times higher in equivalent width (though $\sqrt{2}$ lower in flux). For the northern jet R2, crossed E-W by the slit to maintain small-scale contrast at the expense of areal coverage, the equivalent-width limits are approximately twice as large, corresponding to roughly 1.5 times higher flux limits.

During these observations, the SIT detector exhibited low-level zero-point instabilities on spatial scales mapping to 100-200 Å. Thus, we cannot provide more detailed spectral-shape information from these data.

2.2. Radio Images

2.2.1. *1.4 GHz Data*

We obtained archival data made with the NRAO[2] Very Large Array in the C configuration on 10 February 1983, at 1465 MHz with 50 MHz bandwidth. There were 261 minutes of on-source time. Images were made, CLEANed, and self-calibrated using the AIPS package, yielding naturally-weighted images with noise levels (near the center of the image) of 7 x 10^{-5} Jy/beam, very close to the theoretical noise of 6.2 x 10^{-5} Jy/beam. This corresponds to 1.7 x 10^{-7} Jy/sq arcsec. Large images were required to span the region of interest. The images have not been corrected for the attenuation of the primary beam which has a FWHM of 30' at 1465 MHz. The FWHM of the synthesized beam was 33"X 16" with position angle 4°,

The field around NGC 1097 is shown in Figure 4, The galaxy itself is shown in Figure 5.

EDITOR: PLACE FIGURE 4 HERE.

EDITOR: PLACE FIGURE 5 HERE.

The small feature to the northeast of the galaxy at position angle 18° is not the elliptical companion NGC 1097A (PA 35°) but is probably a background source seen through the optically thin disk of NGC 1097,

---

[2]The National Radio Astronomy Observatory is operated by Associated Universities, Inc. under contract with the National Science Foundation.

We did not detect emission from the jets in the 1.4 GHz images. The limits and their implications for jet processes are discussed in Section III and IV.

2.2.2. 327 MHz Data

New observations at lower frequencies were also obtained, using the P band at 327 MHz at the VLA. These data were mapped using experimental three-dimensional FFT and CLEAN programs developed by T.J. Cornwell. Three-dimensional transforms and beam shapes are necessary due to the large sky curvature over the primary beam area of a VLA antenna at 327 MHz (the half-power beamwidth there being about 2.5°). The observations were made at night to minimize ionospheric effects; we observed on three separate nights (23, 25, 26 October 1989) but found that the data for the best night was better than data combined for all three nights. The total observing time was 12 hours (4 hours per night) obtained while the VLA was in a hybrid C/D array. The bandwidth was limited to 3.125 MHz to avoid man-made interference,

EDITOR: PLACE FIGURE 6 HERE.

The resulting image (Figure 6) has a confusion-limited noise level of 1 mJy/beam, consistent with other 327 MHz images from that epoch. The expected thermal noise was 0.2 mJy/beam. There is evidence of systematic calibration errors which vary over the image. The most obvious errors are shifts in the positions of some, but not all, sources when the dirty and deconvolved images are compared. The phase errors responsible for these shifts are most likely due to the ionosphere. If the isoplanatic patch due to ionospheric phase variations is smaller than the area imaged, the result will be baseline-dependent errors which standard self-calibration cannot remove. At 327 MHz, the isoplanatic patch size could be much smaller than our field of view. Schwab (1984) has considered techniques

for imaging over multiple isoplanatic patches, but this is difficult because of the need to determine multiple gain solutions per antenna during each solution interval.

The galaxy itself is detected at the 1.05 Jy level (Figure 6). The galaxy image is partially resolved by the 150 x 150 arcsecond synthesized beam. Although a large number of sources appear in the 327 MHz VLA field, there is no indication that any of them are associated with the NGC 1097 jets. We see no evidence for extended emission which could be associated with "fossil" radio lobes near or beyond the ends of the optical jets. The observations did detect extended emission associated with a group of distant galaxies 80 arcminutes to the southeast (P. A. $\sim$ 150°) of NGC 1097. Figure 7 shows the central region of our 327 MHz image, covering an area approximately twice as wide as the extent of the optical jets. No emission associated with the jets is detected.

EDITOR: PLACE FIGURE 7 HERE,

3. Analysis

3.1. Optical Morphology

As was clear from the earliest detection of the jets (Wolstencroft and Zealey 1975), they have very low surface brightness, less than 1% of the night-sky brightness at a good ground-based site. Accordingly, on the normally reduced CCD frames only their brightest portions are visible, Structures large compared to the seeing disk or pixel size may be enhanced by smoothing or more elaborate spatial filtering, and indeed Gaussian smoothing was found very effective in tracing the jet structure,

The southern jet R4 is not visible on the original or Gaussian-convolved B images (not shown), being lost against the strong gradient in starlight. Jet R4 is much fainter than

its nearly opposite counterpart R2, which is 0.9 magnitudes brighter in peak B surface brightness and clearly detected with only half as much integration time.

Spatial filtering of the images was used to address the nature of the condensations or knots present along the dogleg jet R1. Detailed comparison of images median-filtered to reject increasing spatial scales indicates, along with the constant color noted above, that the knots are parts of the dogleg jet. Otherwise, they would either need to be elongated along the jet or occur in "holes" in the jet itself. Thus the condensations are integral to the jet structure. All three jets observed are somewhat curved with the curvature of jet R2 being most noticable. The jets themselves vary in length from about 5'to 19' (Lorre 1978); this translates to projected sizes of 19 to 70 kpc. A typical jet width of about 15" corresponds to about 920 parsecs.

3.2. Optical Colors and Spectroscopy of Jets RI and R2

Color measurements can be made on portions of the jets larger than about 5 arcseconds in size. The two jets (R1 and R2) imaged in both B and V bands are bluer than the night sky, in agreement with Lorre's (1978) results. More quantitatively, the colors have been measured by summing the full width of the jets after removing faint stars and cosmetic defects via median filtering. Color and intensity profiles along jet RI and the "dogleg" are shown in Figure 8.

EDITOR: PLACE FIGURE 8 HERE.

The color is constant within the errors, including both prominent condensations observed spectroscopically, with $B - V = 0.45 \pm 0.1$ (typical of FO stars). No color trend is apparent either radially outward from the galaxy or along the "dogleg" portion of the jet.

Our optical spectra of the two brightest condensations in the dogleg jet show no emission lines: they are not HII regions.

3.3. 1.4 GHz Radio Morphology of NGC 1097 and Immediate Environs

The 1.4 GHz radio images show the disk of the barred spiral NGC 1097 and about 65 unresolved and slightly resolved objects which are probably background objects. We find no evidence of extended structure associated with the optical jets, nor do we find an overabundance of radio sources in the field. The 20-cm radio structure of the galaxy itself matches the optical structure in general: a barred spiral structure with two outside spiral arms, The peak in the radio emission trails the optical emission in the bar, assuming the galaxy rotates in the direction implied by the arms, The radio emission is strongest where the H-α image shows HII regions, including a strong nuclear peak of 120 mJy/beam. The tattered end of the spiral arm in the west near NGC 1097A has many HII regions and shows considerable radio emission. Lacking matched-resolution data at another radio frequency, we are unable to separate the thermal and non-thermal contributions to the 20-cm emission.

There is no indication that the 20-cm radio emission from the outer galactic spiral arms is disturbed at the position angles of the optical jets. Any gross discontinuities might have signalled enhanced absorption or emission. The disk radio emission is somewhat clumpy, following as it does the distribution of HII regions seen in $H\alpha$. The significance of the very small changes in surface brightness is not clear.

3.4. 1.4 GHz Radio Number Counts in the NGC 1097 Field

The number of radio sources on the image is consistent with the number expected from radio source counts: Mitchell and Condon (1985) find 63 sources within a 34' diameter

field above 0.35 mJy, our 5-a detection limit. Wewould have easily detected a supergiant HIIregionlike30 Doradus, forwhich the(thermal plus nonthermal) flux density would be about 1.6 mJy and the size about 16", but we would not have detected the small, faint type of HII region common in the Orion star formation complex for which the expected flux density would be of order 0.63 μJy.

In checking to see if there was any extended radio emission associated with the optical jets, we drew four lines on our radio image along the position angles of the optical jets as given by Lorre (1978): 54°, 15°, 195°, and 223° for RI, R2, R3, and R4, respectively. In doing so, we noticed that there were ten radio features within 5 degrees of the optical jets' position angles. Three of these objects are about as bright as 30 Doradus would be at the 12.3 Mpc distance of NGC 1097; two others are much brighter (respectively: 1.9, 1.3, 1.3, 12.0, and 5.7 mJy). Having divided the region around NGC 1097 into 36 bins of 10 degrees each, and counting the 65 reliable detections (excluding the galaxy itself) on the image, it is not surprising that all four bins associated with the optical jets contain radio sources. In four bins of 10° each, chance will place 7 or 8 sources; the optical jet bins contain 10 sources. If the ten radio sources were supergiant HII regions, they would have strong optical emission lines which might be detectable on the H-alpha plate taken by Arp (cited in Wolstencroft 1981) but no emission-line features were seen in the jet. Arp, Wolstencroft and He (1984) have searched two objective prism plates for emission-line objects: none of their 43 candidates have any radio counterpart on our 20-cm image, consistent with the relative rarity of radio-bright objects among optically selected quasars.

4. Discussion

The nature of the features in NGC 1097 has been debated since their discovery. We discuss here the implications of our data for interpretations as aging synchrotrons sources,

star formation at the edges of ejected cones of material, and unusually aligned tidal tails.

The best-attested examples of ejects from galactic nuclei are the synchrotrons jets found in radio galaxies (and some quasars). A few of these are detectable in optical light, by the most energetic tail of the synchrotrons spectrum which is most powerful at low frequencies. Known examples of radio jets which are detectable in the visible (3 C273, M87) have spectral indices between radio and visible frequencies of-0.6 to -0.9, typical of optically thin synchrotrons emission and consistent with extrapolations of the spectral indices at high radio frequencies (in some cases with evidence for a break at high frequencies, steepening the local index in the optical range). For the jets of M87 and 3C273, there is good evidence that the visible emission is synchrotrons radiation coming from the same population of relativistic electrons as the radio emission. In contrast, the radio-optical spectral index for the jets of NGC 1097 is ≥ 0. This rules out a common synchrotrons source unless highly implausible absorption mechanisms are invoked to explain the lack of strong radio emission at 20 and 92 cm.

The fossil radio lobes that would mark an old synchrotrons source could have faded over time due to adiabatic expansion. For example, expansion by a factor of two in radius would cause the lobes to appear fainter by a factor of 32 (Moffet 1975). However, this still implies that the initial surface brightness of the lobes was small. Assuming a total radio lobe area of 50 square arcminutes (comparable to the area enclosed by each pair of visible jets) the initial total radio flux density at 92 cm would have been less than 20 mJy. This is extremely weak compared to the lobes of nearby "active" radio galaxies. Coupled with the (almost) total lack of double sources among genuine spiral galaxies, these arguments make an origin for the jets of NGC 1097 in the same kind of ejection seen in radio galaxies and their jets very difficult to support.

As Carter et al. (1984) showed, the broad-band colors of the jets can be accounted

for by starlight. We find that this statement can restrengthened byadding an additional optical band to their single-wavelength observations, as well as their near-IR aperture photometry. Whether the stars were formed by the passage of nuclear ejects or in some tidal event, the colors may be used to estimate the age of the features. If the stars were formed in a brief burst, an age estimate is possible based on continuum colors and starburst models (we take those of Newberry, Boroson, and Kirshner 1990 for definiteness). The observed B-V and a local IMF slope imply a burst age 6 x 10^8 years, This is much larger than the age found by Arp (1976) from assuming the jets to have caused disruptions in the spiral arms. The colors of both R1 and R2 are considerably bluer (B-V= 0.45) than the color integrated over the main disk of NGC 1097, for which B-V = 0.85, U-B=0.43 (Wray 1988). Such blue colors (and the implication of recent star formation) are typical of "plume" and "tail" tidal features of the interacting galaxies studied by Schombert, Wallin and Struck-Marcell (1990).

From our very deep optical images of the dogleg jet **RI** and jets **R2** and **R3, we** find that the optical jets are not simple linear structures: they are both curved and clumpy. The right-angle bend of R1 is especially difficult to explain in an ejection picture, while relatively sharp bends in projection are not unknown in tidally interacting systems. The dogleg jet contains condensations which resemble dwarf galaxies in color, absolute magnitude, and linear dimensions. Jet feature R2 is thin and slightly curved toward the northwest; the curvature is most marked near the galactic disk. The disk and spiral arms of the galaxy do not appear to be disturbed at the position angles of the three jets studied (though see Arp 1976 for a dissenting opinion from Hα imagery near R2).

The narrowness of the jets and large implied ages for the stellar population mean that the observed stellar population must have a small velocity dispersion along at least one direction. A typical jet profile is nearly Gaussian in projection, with σ = 750 pc. If the

jet is composed of stars at the single-burst age of 6 x 10^8 years estimated above, only for stellar velocity dispersions $\sigma < 1.5$ km s^{-1} would the jets remain so narrow. While an observational selection would certainly operate against detecting any component blurred by a much larger velocity spread, an important portion of the hypothesized stellar population formed in the jets would have been surprisingly cool (in the dynamical sense). This argues for a tidal origin, since features produced by impulses acting on disks remain very cool and narrow in at least one dimension (as in some of the vary narrow tidal tails seen in the Arp (1966) atlas).

Numerical modelling of interactions between low-mass companions and non-spherical galaxies by Hernquist and Quinn (1989) generated a wealth of possible post-collision morphologies. The companion galaxy is shredded by the encounter, leaving delicate traceries or "shells" whose appearance changes with viewing angle. Some of the models presented by Hernquist and Quinn certainly have strong X-shapes when viewed along principal axes (see, especially, their Figure 8), though the profiles of the features in NGC 1097 mean that they must be more like true near-linear features in three dimensions than conical structures seen edge-brightened.

A useful comparison for a tidal interpretation comes from the jet or tail of NGC 4651, as shown in Sandage, Veron, & Wyndham (1975) and in the Arp (1966) atlas. We are unaware of any subsequent detailed study, though much work has been done on the cluster of galaxies around the QSO 3C 275.1 which lies only 1.8 arcminutes south of the "jet" feature. Schneider & Corbelli (1993) show a deep B image of the feature, which exhibits a diffuse turn to the south much like feature R1 in NGC 1097. They report no H I emission from the feature to a 3-u limit of 10^{19} atoms cm^{-2}. The linear scale, width, and slightly flaring form are comparable to the jets of NGC 1097, especially R2. Photometry from BVR images taken with the ESO 3.6m telescope and EFOSC system shows that it is both

brighter and bluer than the NGC 1097 features. The central surface brightness of the NGC 4651 galaxy envelope is B = 24.02 and V = 23.96 per square arcsecond, 1.7 magnitudes brighter than jets RI and R2 in NGC 1097. The implied color B - V = 0.06 is significantly bluer than found in NGC 1097, and for a single-burst stellar population suggests an age of order 3 x 10^7 years, from the burst models of Bruzual & Charlot (1993). Compared to the dynamical age of any feature of this linear extent at typical galaxy velocities, this means that many of the stars must have formed *in situ*, as is known to happen in at least some tidal tails from the presence of H II regions (in, for example, NGC 4676 and NGC 4038). The fading in V surface brightness that should accompany a reddening from B - V = 0.06 to 0.4 would be about 3.5 magnitudes, so that, if a simple burst population is present in both, the tail in NGC 4651 actually requires a smaller stellar mass surface density (by about a factor five) than the NGC 1097 features. The comparison is especially interesting because a stronger case can be made for a tidal origin in NGC 4651. The feature is not quite straight, with an overall curvature and small oscillations in the ridgeline location, and not quite radial; a projection of the mean centerline passes about 28 arcseconds north of the nucleus (projecting to 2.4 kpc on the plane of the sky if we take NGC 4651 to be at a Virgo-cluster distance of 18 Mpc). This is so large that no plausible connection to the nucleus exists. The colors are reasonable for a (rather young) stellar population, and the total brightness ($V \approx 15.6$, $M_V = -15.5$) is appropriate for either a small amount of material stripped from the disk of NGC 4651 or for a former dwarf companion. Individual, nearly linear tails are well known, and an obvious surface-brightness selection effect operates in favor of seeing curved features as linear in their own plane (as in NGC 4676 and Arp 295). Especially in view of the 90° bend near the tip of the NGC 4651 feature, we feel that the analogy strengthens the case for the NGC 1097 "jets" being an unusual set of tidal tails.

5. Conclusions

By comparing our optical and radio images, we have shown that there is no 1.4 GHz radio emission associated with the optical jets in NGC 1097 on angular scales of 15"-30" with a 3-σ detection limit of 2 x 10^{-4} Jy/beam or about 5 x 10^{-7} Jy per square arcsecond. This limit is fainter than previous results (HHK and WTP). Our 327 MHz radio images show no extended emission near the ends of any of the optical jets.

Based on the optical and radio imaging presented here, we believe it is unlikely that the optical jets of NGC 1097 were formed directly or indirectly from the ejection of matter from an active galactic nucleus. The optical emission from the jets originates in stars, possibly torn from the main body of the galaxy through tidal interaction with NGC 1097A. Although tidal models seemed unlikely when we began this work, we must reconsider them after eliminating the other possibilities. As detailed in section 4, we find that the balance of evidence is best accounted for if these are indeed an unusual set of tidal features.

An X-shape of tidal remnants requires special viewing conditions. It is thus of considerable interest to know how common galaxies with these features are. An optical search for other objects with optical jets has been undertaken by WCK. This search was based on experience gained while surveying previously reported jet-like features (Keel 1985), and was thus designed to reject, as far as possible, tidal tails and similar interloping phenomena. The search was carried out on glass copies of the SRC J survey plus confirming CCD imagery, and was sensitive enough to have found the jets of NGC 1097 independently. Full details will appear elsewhere, but the following results are directly relevant: No other bright galaxy shows a similar system of features at this surface brightness, and the few spirals with linear, radial features (eg., NGC 4651) do not show the multiple features seen in NGC 1097. This interacting spiral galaxy with four optical 'jets" is still a *rara avis* of the celestial menagerie.

We acknowledge useful discussions with Ray Wolstencroft and Jack Sulentic. We are grateful to Tim Cornwell for access to his three-dimensional deconvolution routines. This work was supported at the California Institute of Technology by grants from the National Science Foundation (AST-85-09822 and AST-88-14544). Part of this research was carried out at the Jet Propulsion Laboratory, California Institute of Technology, under contract with the National Aeronautics and Space Administration. WCK acknowledges support from EPSCOR grant RII-8610669.

REFERENCES

Arp, H. 1966, ApJS, 14, 1. (Arp Atlas)

Arp, H. 1976, ApJ, 207, L147.

Arp, H., Wolstencroft, R. D. and He, X.T. 1984, ApJ, 285, 44.

Baum, S.A. and Heckman, T. 1989a, ApJ, 336, 681.

Baum, S.A. and Heckman, T. 1989b, ApJ, 336, 702.

Bruzual, G. A., & Charlot, S. 1993, ApJ, 405, 538.

Carter, D., Allen, D.A. and Malin, D.F. 1984, MNRAS, 211, 707.

Graham, J.A. 1982, PASP, 94, 244.

Hernquist, L. and Quinn, P. 1989, ApJ, 342, 1.

Hummel, E., van der Hulst, J. M., and Keel, W.C. 1987, A&A, 172, 32,

Keel, W.C. 1985, AJ, 90, 2207.

Lorre, J. 1978, ApJ, 222, L99.

McCarthy, P., van Breugel, W., Spinrad, H. and Djorgovski, S. 1987, ApJ, 321, L29.

Mitchell, K.J. and Condon, J.J. 1985, AJ, 90, 1957.

Moffet, A.T. 1975 in Stars and Stellar Systems, ed. A. Sandage, M. Sandage, J. Kristian (University of Chicago Press: Chicago), 211.

Newberry, M. V., Boroson, T.A. and Kirshner, R.P. 1990, ApJ, 350, 585.

Ondrechen, M. P., van der Hulst, J. M., & Hummel, E. 1989, ApJ, 342, 390.

Sandage, A., Veron, P., & Wyndham, J. 1965, ApJ, 142, 1307.

Schneider, S.E. & Corbelli, E. 1993, ApJ, 414, 500.

Schombert, J. M., Wallin, J. F.. & Struck-Marcell, C. 1990, AJ, 99, 497.

Schwab, F. R. 1984, AJ, 89, 1076.

Storchi-Bergmann, T., Baldwin, J. A., & Wilson, A.S. 1993, ApJ, 410, L11.

Storchi-Bergmann, T., Eracleous, M., Livio, M., Wilson, A. S., Filippenko, A. V., & Halpern, J.P. 1995, ApJ, 443, 617.

Wolstencroft, R.D. 1981, Proc. of the Second ESO/ESA Workshop, Munich, ESA-SP-162, March 1981.

Wolstencroft, R.D. and Zealey, W. J. 1975, MNRAS, 173, 51p.

Wolstencroft, R. D., Tully, R. B. and Perley, R. A. 1984, MNRAS, 207, 889.

Wolstencroft, R. D., Ku, W. H-M., Arp, H. and Scarrott, S.M. 1983, MNRAS, 205, 67.

Wray, J.D. 1988 Color Atlas of Galaxies (Cambridge University Press: Cambridge)

This manuscript was prepared with the AAS LaTeX macros v4.0.

Fig. 1.— Blue-light image of NGC 1097, enlarged from ESO SRC J Plate. The original negative for the survey image was taken with the U.K. Schmidt Telescope, and is copyright SRC J Survey. Fields of CCD images are outlined.

Fig. 2.— CCD image (V filter) of northeast jet R1. The locations of the spectroscopically observed condensations are (x=150, y=260) pixels and (x=265, y=140) pixels.

Fig. 3.— a) CCD image (V filter) of north jet R2. b) Same image after convolution with a 5“ Gaussian filter.

Fig. 4.— Radio image of NGC 1097 field at 1.4 GHz. The peak brightness was 0.121 Jy/beam. Contour levels are (4, 8, 16, 32, 64, and 128) x (7x 10^{-5}) Jy/beam. The FWHM of the synthesized beam was 33”X 16” with position angle 4°.

Fig. 5.— Radio image of NGC 1097 at 1.4 GHz. The peak brightness was 0.121 Jy/beam. Contour levels are -0.25,0.25, 0.5, 1, 2,4,8, 16, 32,64, and 120 mJy/beam. The FWHM of the synthesized beam was 33”X 16” with position angle 4°,

Fig. 6.— The full 327 MHz VLA field of view centered on NGC 1097. Contour levels are -1, 1, 2, 4, 8, 16, 32, 50, 70, and 95% of the peak brightness (1.046 Jy/beam). The restoring beam is a circular Gaussian with FWHM = 150 arcseconds. The image has not been corrected for primary beam attenuation. The apparent change in noise level with distance from the center is caused by the primary beam response.

Fig. 7.— The central 1° x 1° region of our 327 MHz VLA image of NGC 1097, This is approximately twice the extent of the optical jets. Contour levels are -1, -0.5, 0.5, 1, 2, 4, 8, 16, 32, 50, 70, and 95% of the peak brightness (1,046 Jy/beam). The restoring beam is a circular Gaussian with FWHM = 150 arcseconds.

Fig. 8.— Color and intensity profiles along the jet R1 and the “dogleg”.

Table 1. Journal of Observations - Imaging

Filter	Exposure	Date	Seeing (FWHM)	Target	AirMass
B	5m+1 0m	28/29 Sept 1983	1.5″	R2	1.01
V	5 x 2m	"	1.4	"	1.00
B	1 0m	"	"	R1	1.00
V	1 0m	"	U	"	1.000
B	3 x 10m	29/30 Sept 1983	1.4	R3	1.05
B	4 x 5 m	"	"	R1 dogleg	1.01
V	4 x 5m	"	"	"	1.00

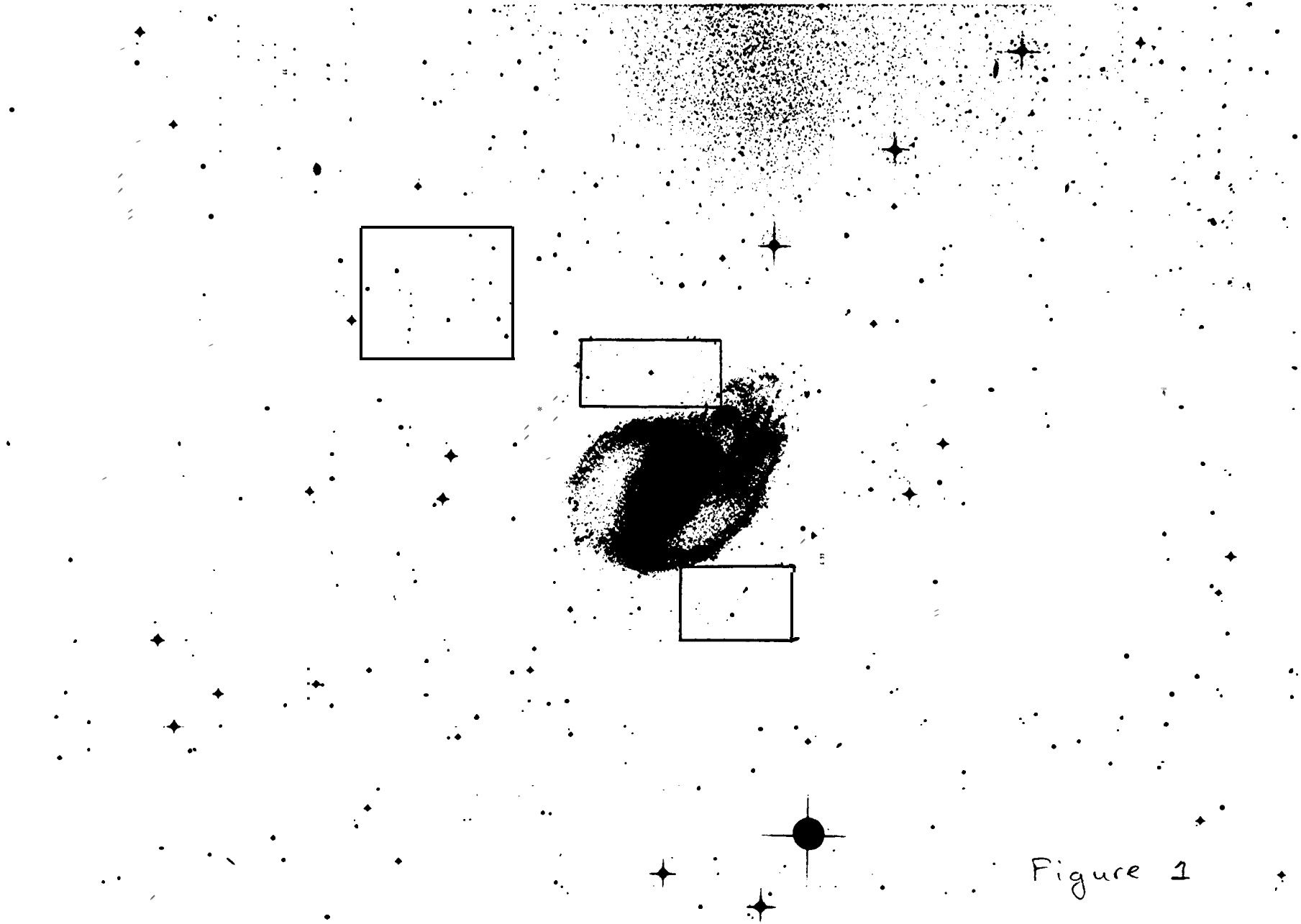

Figure 1

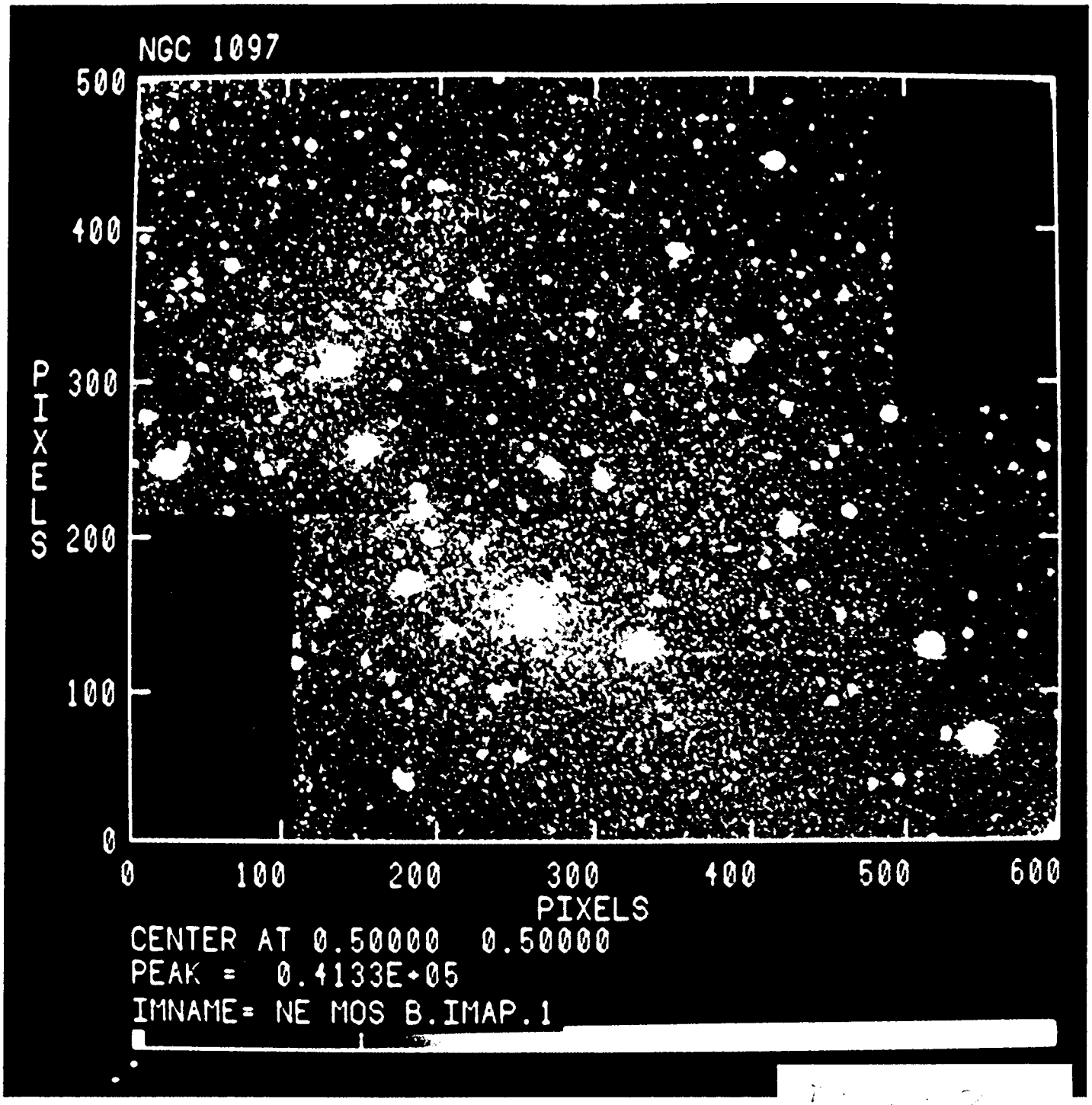
NGC 1097
500
400
300
200
100
0
PIXELS
0
100
200
300
400
500
600
PIXELS
CENTER AT 0.50000 0.50000
PEAK = 0.4133E+05
IMNAME= NE MOS B.IMAP.1

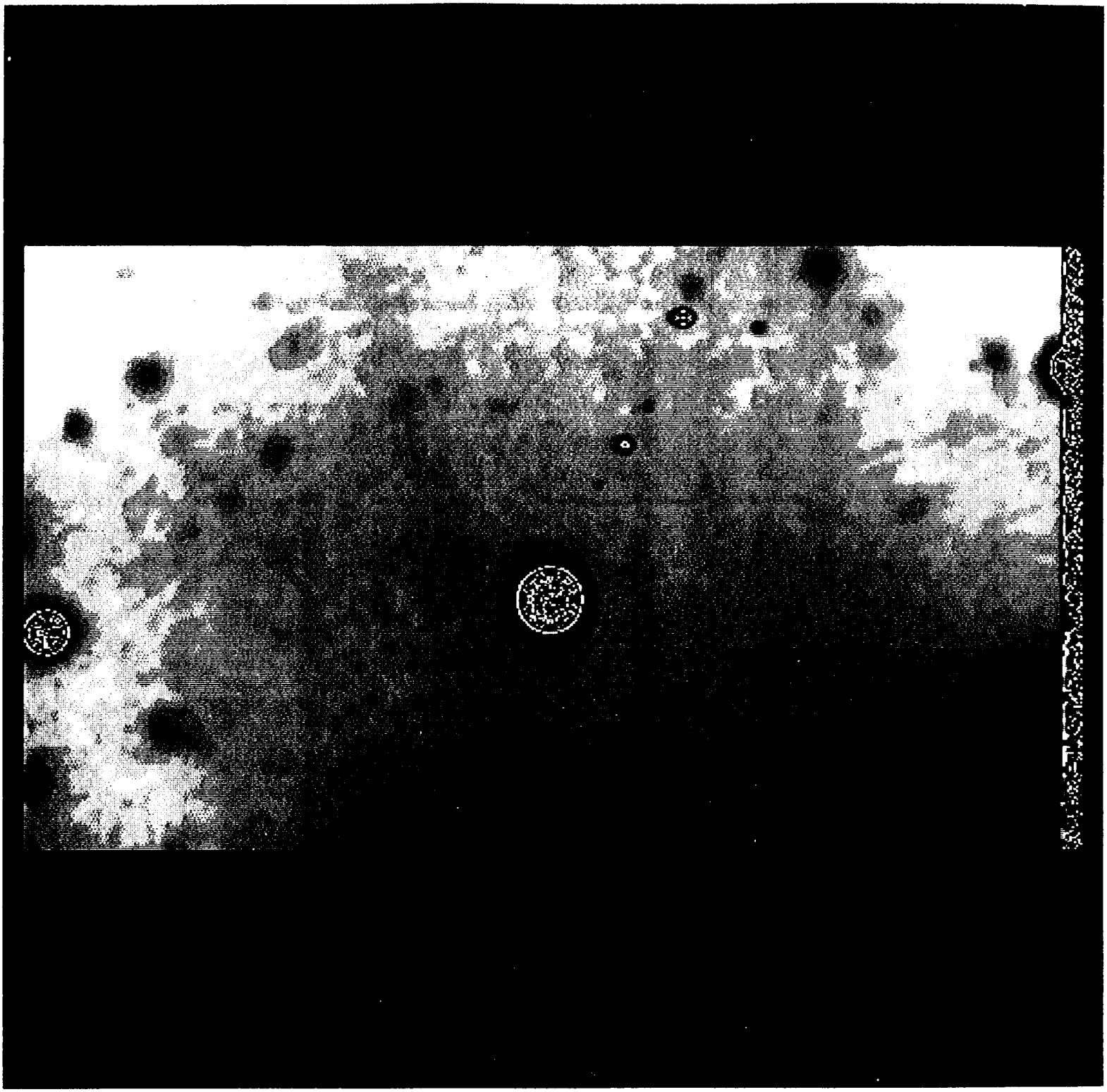

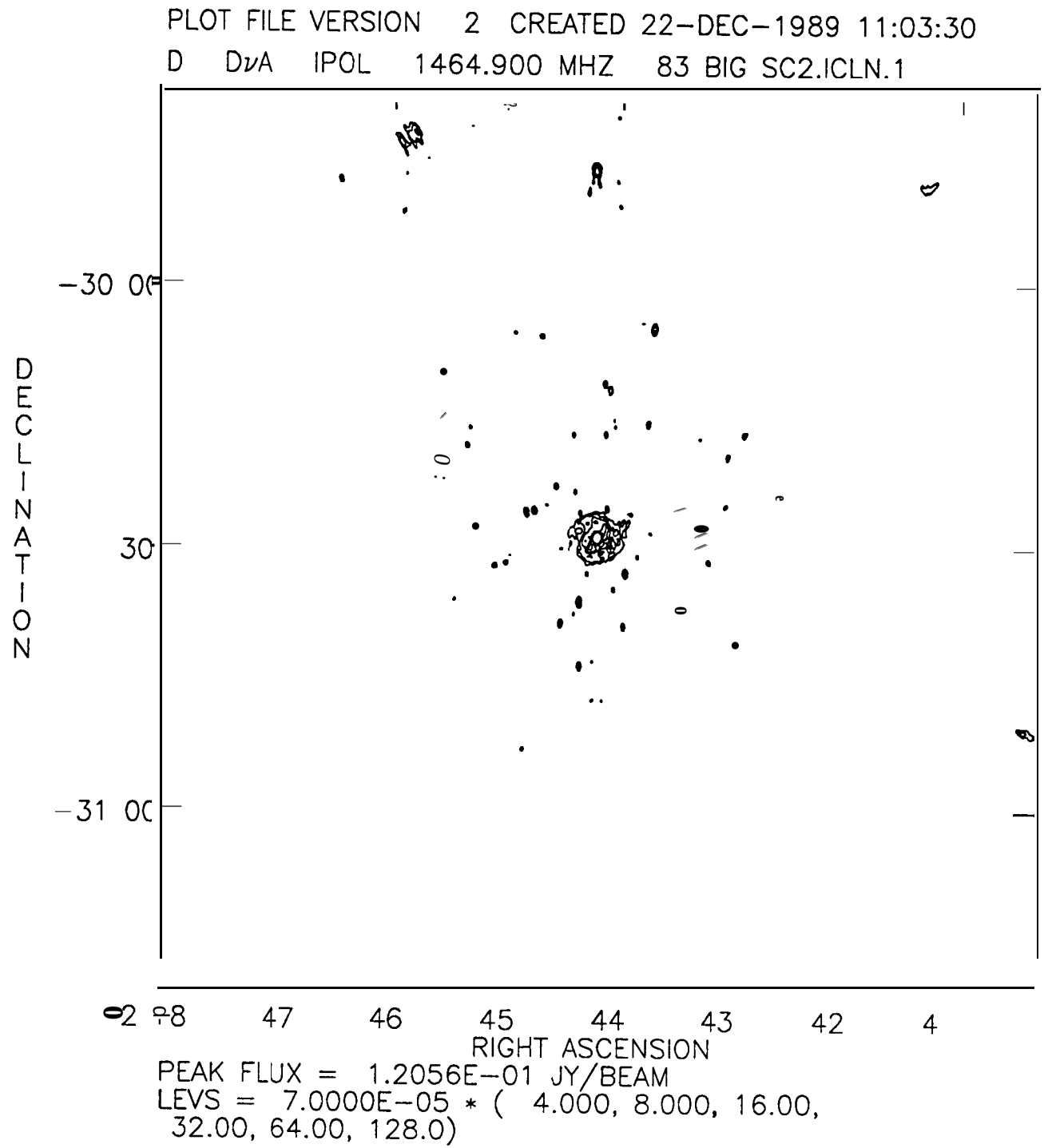
PLOT FILE VERSION 2 CREATED 22-DEC-1989 11:03:30
D DνA IPOL 1464.900 MHZ 83 BIG SC2.ICLN.1
-30 0(
30
-31 0(
DECLINATION
47
46
45
44
43
42
RIGHT ASCENSION
PEAK FLUX = 1.2056E-01 JY/BEAM
LEVS = 7.0000E-05 * (4.000, 8.000, 16.00,
32.00, 64.00, 128.0)

Figure 4

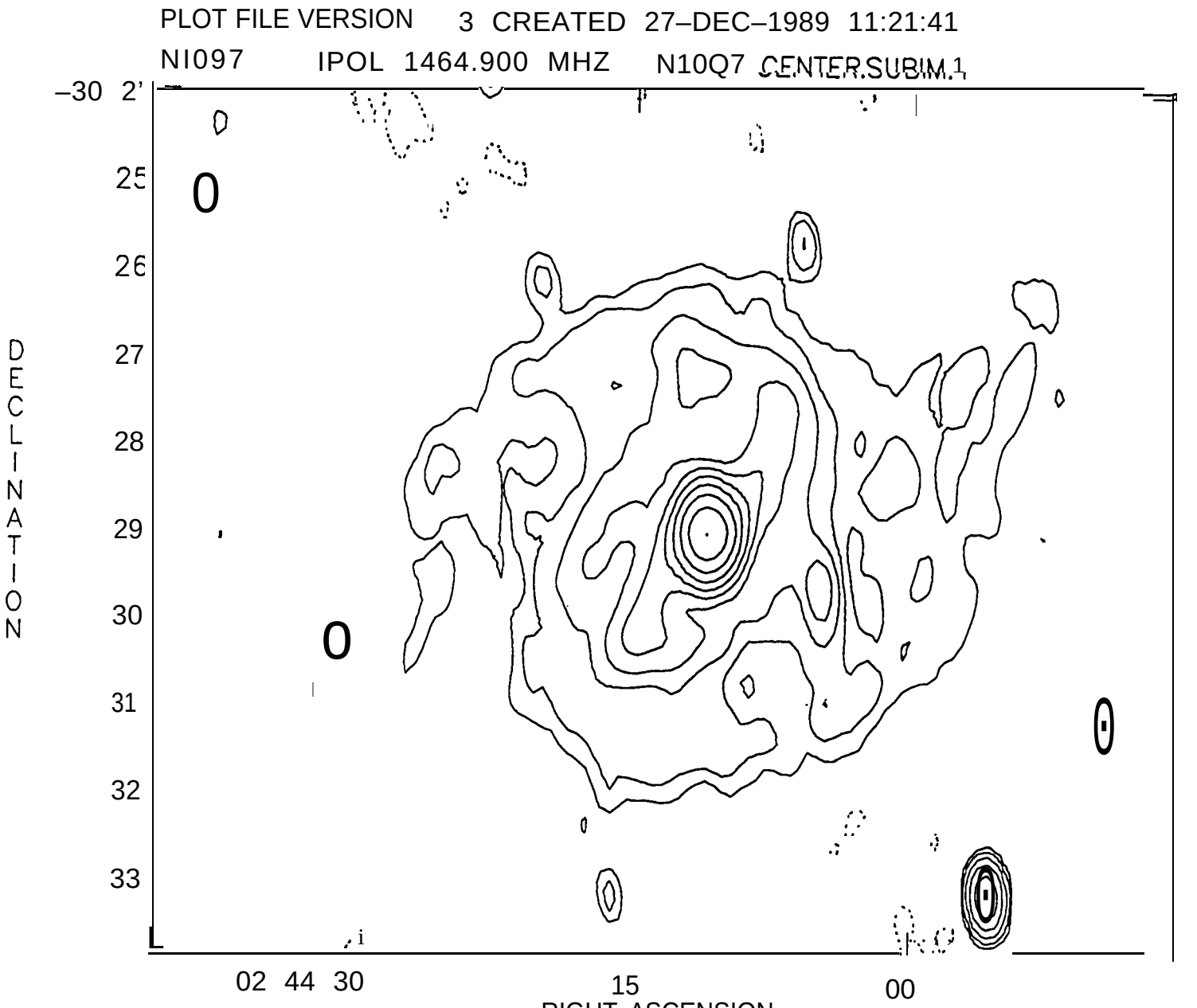
PLOT FILE VERSION 3 CREATED 27–DEC–1989 11:21:41
NI097 IPOL 1464.900 MHZ N10Q7 CENTER.SUBIM.1
–30 2'
25
26
27
28
29
30
31
32
33
DECLINATION
02 44 30
15
00
RIGHT ASCENSION
PEAK FLUX = 1.2056E–01 JY/BEAM
LEVS = 1.0000E–03 * (–0.250, 0.250, 0.500,
1.000, 2.000 4.000, 8.000, 16.00, 32.00,
64.00, 1 20.0)

Figure 5

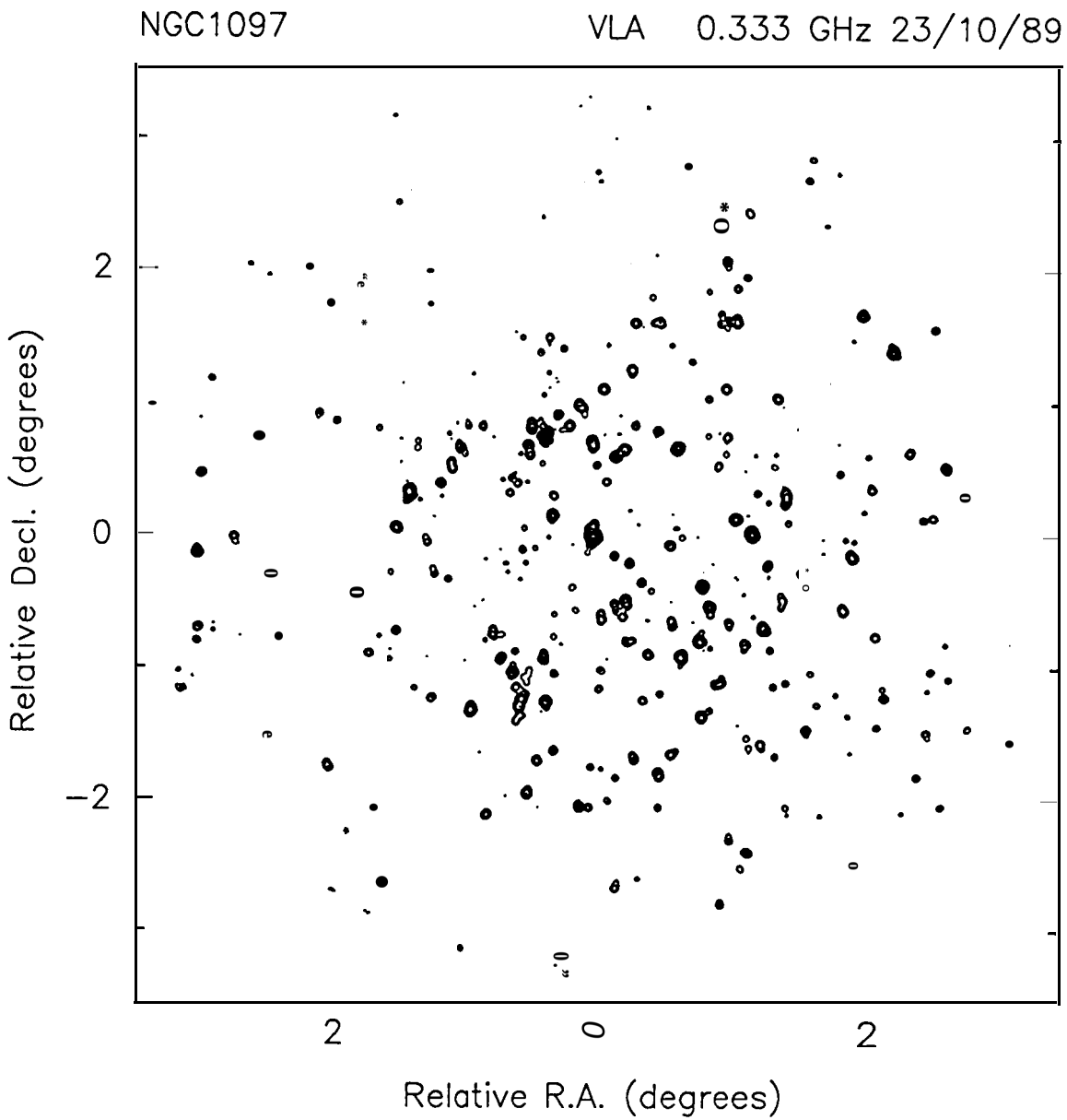

Figure 6

Maximum: 1.046 JY/BEAM
Contours (%): −1.00 1.00 2.00 4.00 8.00 16.00 32.00 50.00 70.00 95.00
Contours (%): 95.00 95.00 95.00 95.00
File: N1097−P.ICLN (28−Nov−1995 11:08)
MAPPLOT (v4.2 − 1992 Jul 6) run by dj [bllac], 28−Nov−1995 14:06:36

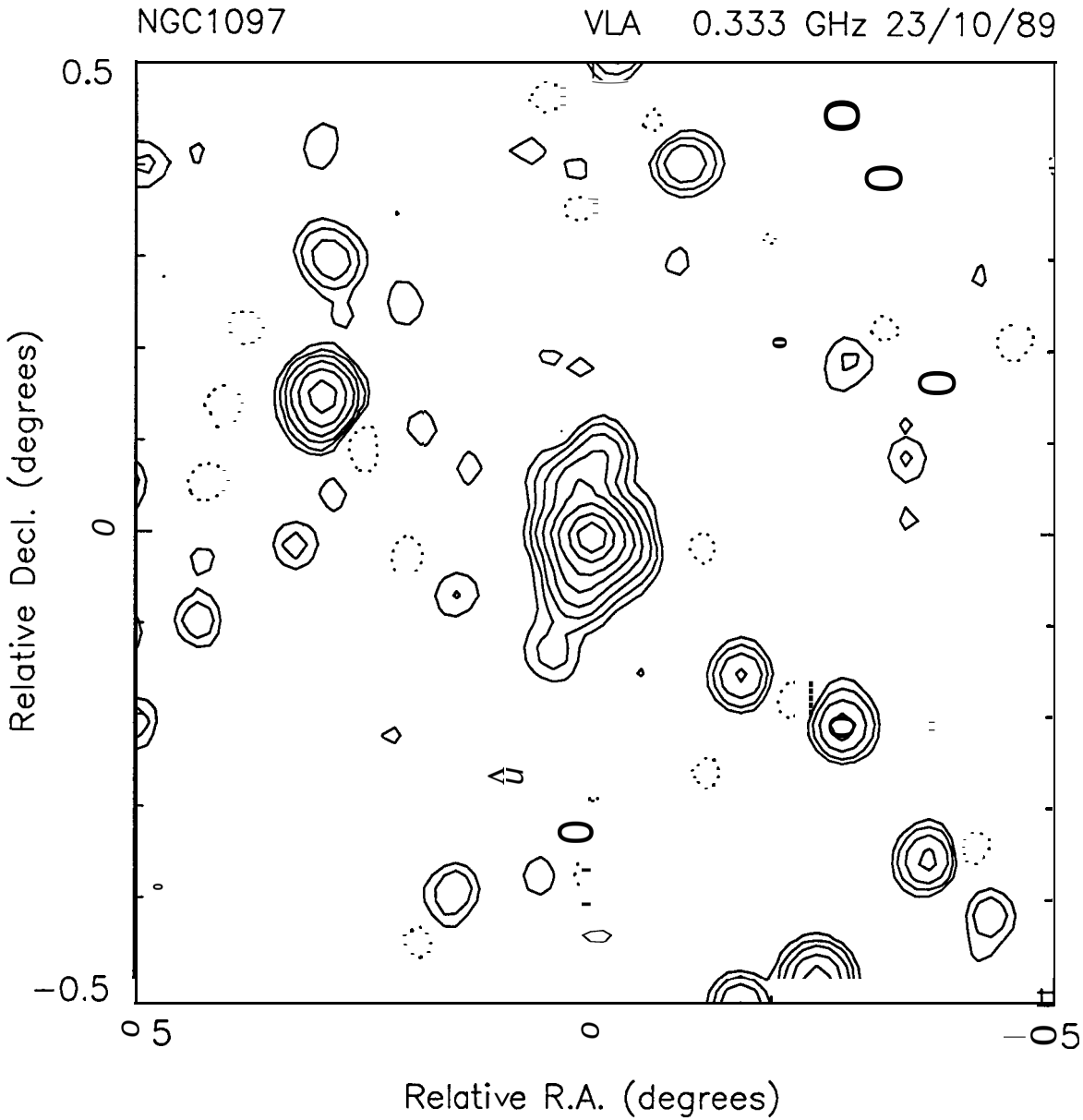

Figure 7

Maximum: 1.046 JY/BEAM
Contours (%): −1.00 −0.50 0.50 1.00 2.00 4.00 8.00 16.00 32.0° 5°.0°
Contours (%): 70.00 95.00 70.00 95.00
File: N1097−P.ICLN (28−Nov−1995 11:08)
MAPPLOT (v4.2 − 1992 Jul 6) run by dj [bllac], 28−Nov− 995 3:48:43

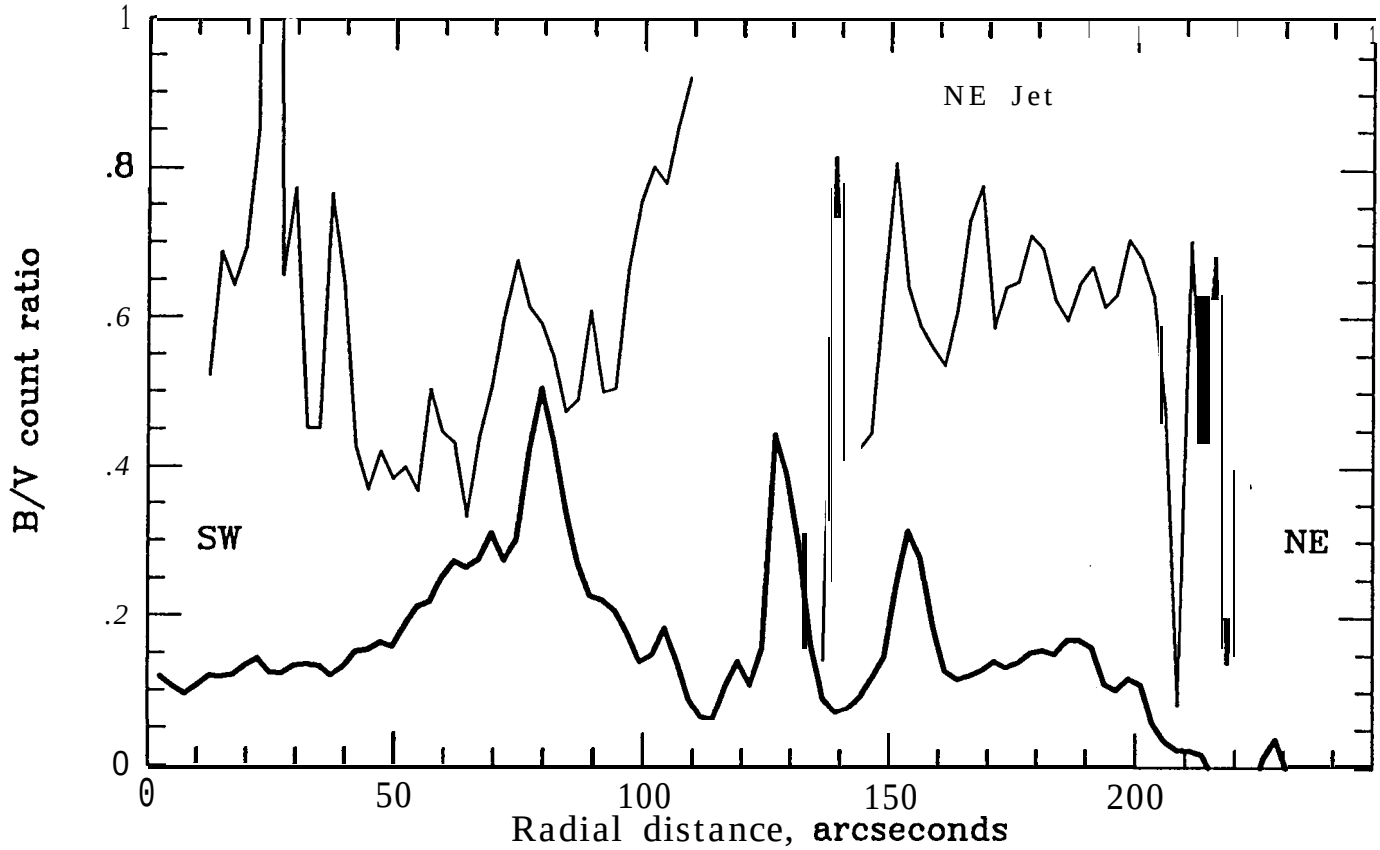
B/V count ratio
1
.8
.6
.4
.2
0
NE Jet
SW
NE
0
50
100
150
200
Radial distance, arcseconds

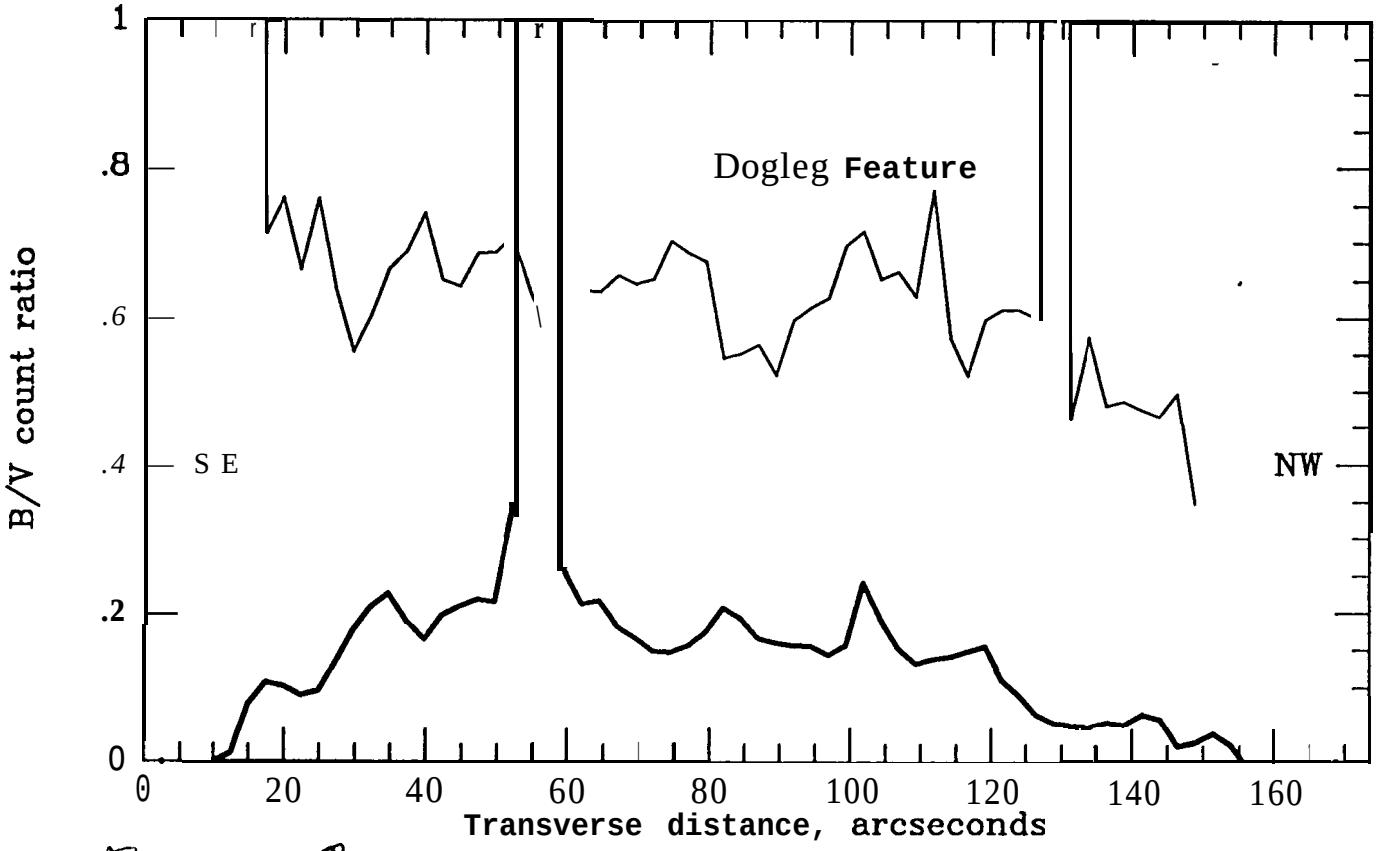
B/V count ratio
1
.8
.6
.4
.2
0
Dogleg Feature
S E
NW
0
20
40
60
80
100
120
140
160
Transverse distance, arcseconds

Figure 8